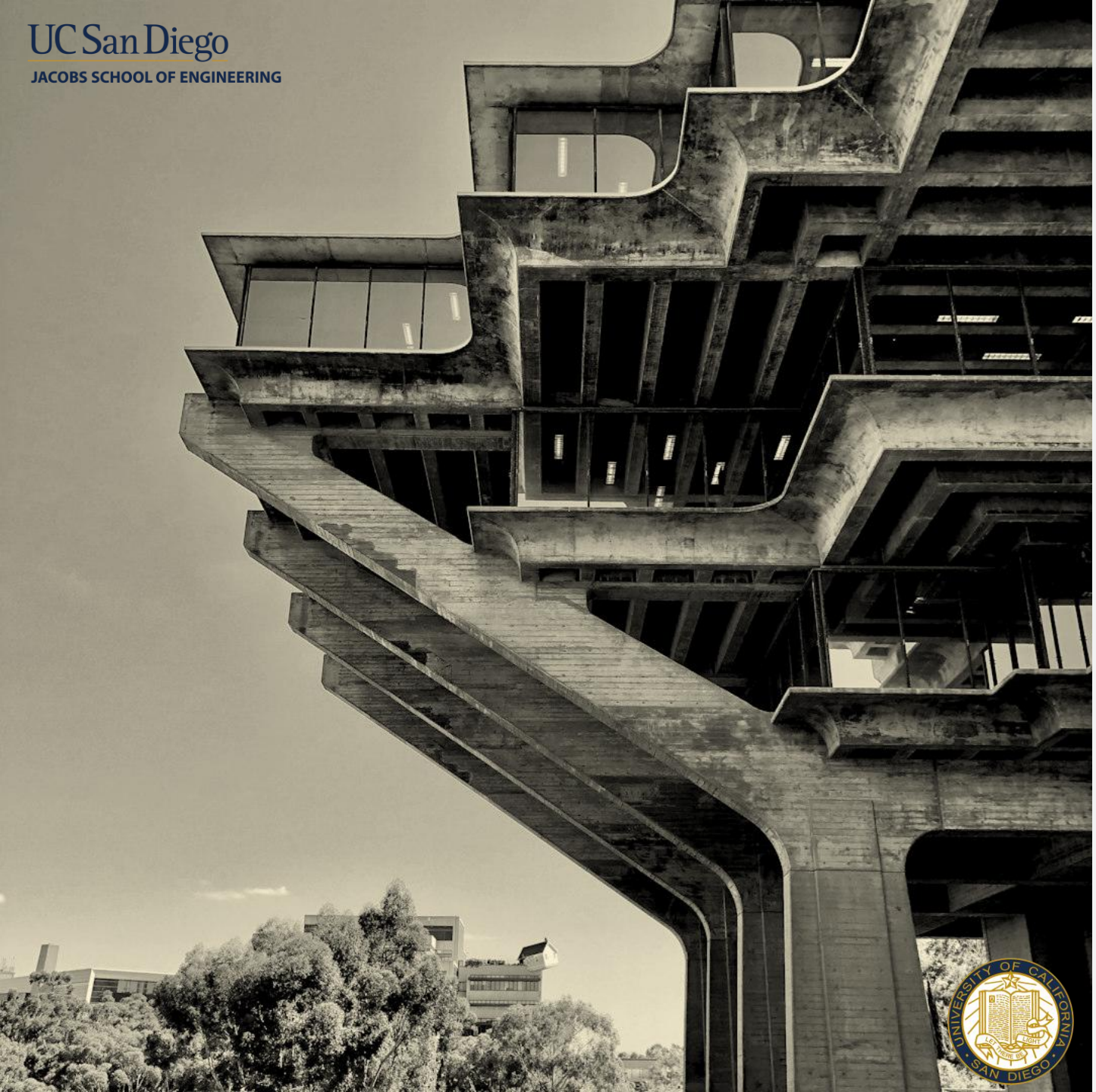

Topology optimization for battery pack design using phase-change materials

Alex Guibert

NASA NESC Webinar

eVTOL vehicles context

Electric vertical takeoff and landing vehicle for urban commuting to

- ✓ Alleviate traffic congestion
  - ❖ American lost on average 99h in 2019 sitting in traffic[1]
  - ❖ 68% of world population in urban areas by 2050 (55% in 2018)[2]

- ✓ Many possible applications: emergency medical services, agriculture, urban air mobility, cargo and delivery services…
- ✓ >1000 concepts[3] proposed including from key players in the industry (Boeing, Airbus, NASA, Bell, Toyota…)

1. INRIX (2019) – Global traffic scorecard
2. United Nation (2018) – World urbanization prospects
3. eVTOL news

eVTOL challenges

- Mass of the batteries and battery pack[1,2,3]
  - Energy density of aviation gasoline (*avgas*) → **45 MJ/kg**
  - Energy density of lithium-ion battery in Tesla → **1 MJ/kg**

  - Internal combustion engine efficiency → **15%**
  - Electric motor efficiency → **60-80 %**

Usable energy

➢ **6.75 MJ/kg vs 0.6-0.8 MJ/kg**

5% vs 25% of total mass[1]

Traditional VTOL → 2000 kg with < 100 kg of fuel

eVTOL → 2500-3000 kg with 700-800 kg of batteries

Brookings (2020)

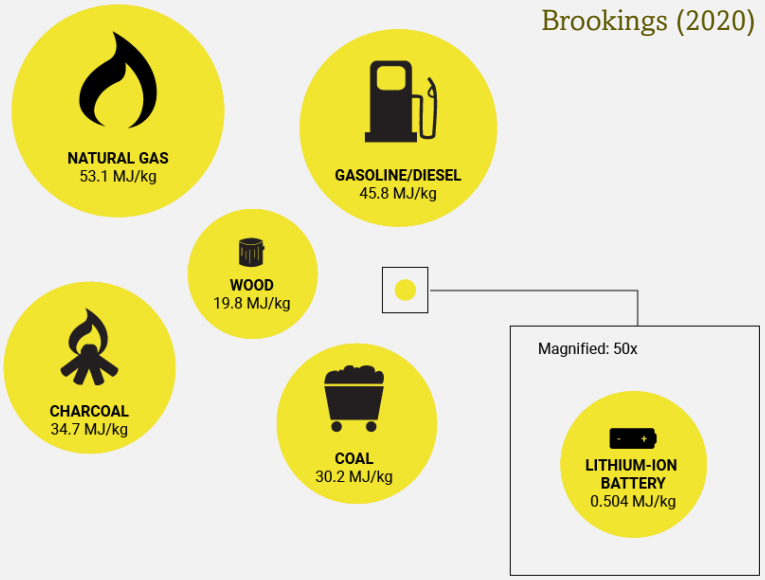

Batteries News (2023)

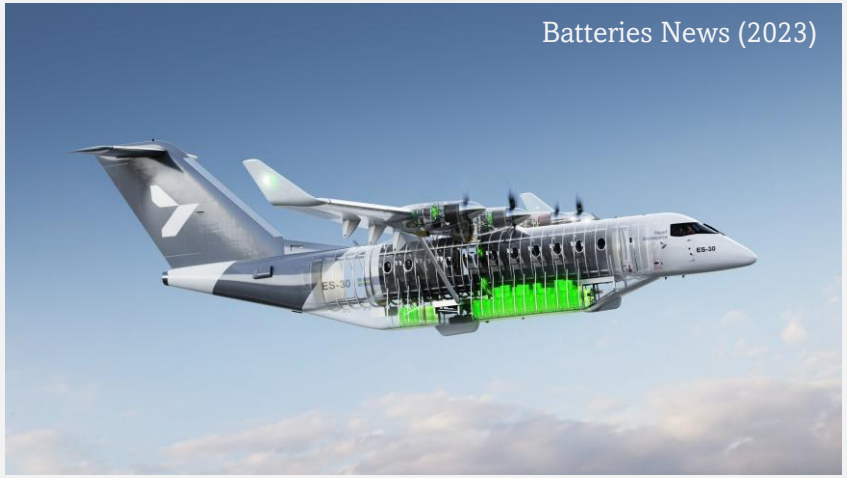

1. Silva *et al.*, "*VTOL urban air mobility concept vehicles for technology development*", AIAA Aviation Conference 2018
2. Fred Schlachter, "*Has the battery bubble burst?*", American Physical Society 2013
3. Battery design, "*Tesla 4680 Cell*"

Battery systems for spacecraft

Ingenuity
6x18650 LiB

Juno
2x55 Ah LiB

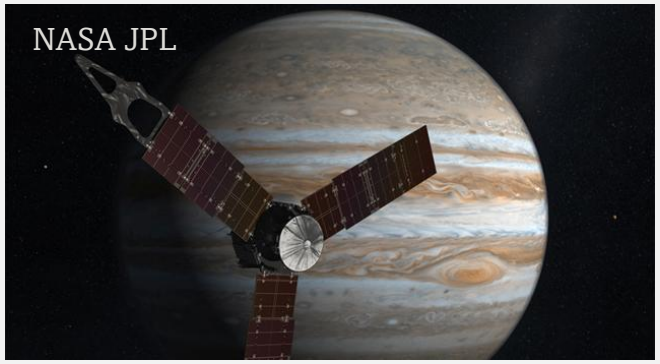

Europa Clipper
LiB system

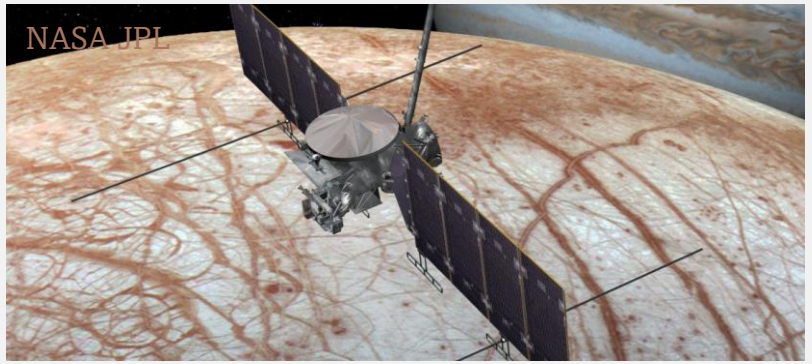

Challenges

- **Temperature variations:** eclipse and load cycles drive large battery temperature variations that can degrade performance and life
- **Safety/reliability:** avoid thermal runaway and keep cells safe for years with no servicing
- **Mass & peak power:** minimize battery mass while still delivering short high-power bursts

A multiscale and multiphysics problem

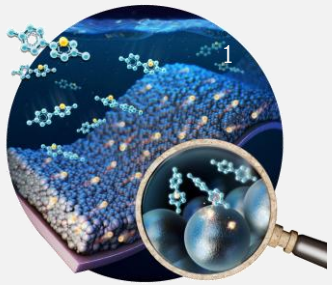

nm

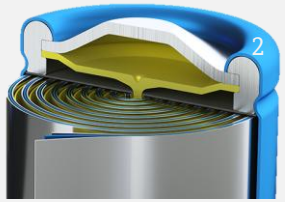

μm

cm

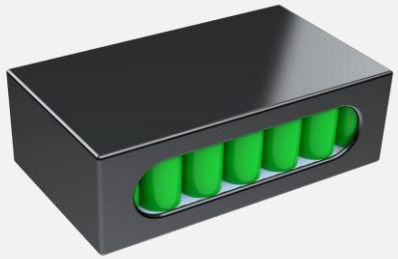

dm

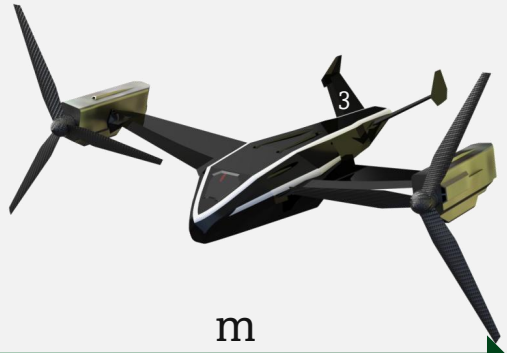

m

heat generation

convective cooling

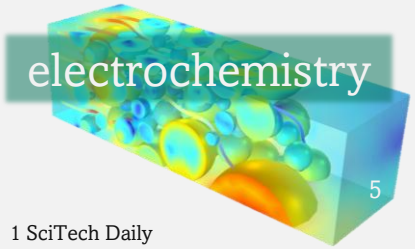

electrochemistry

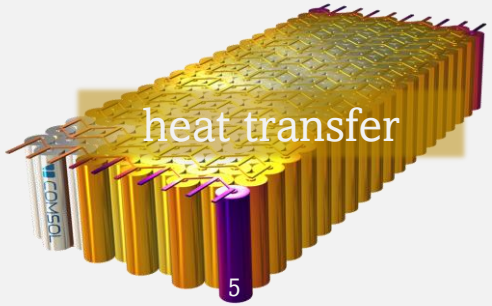

heat transfer

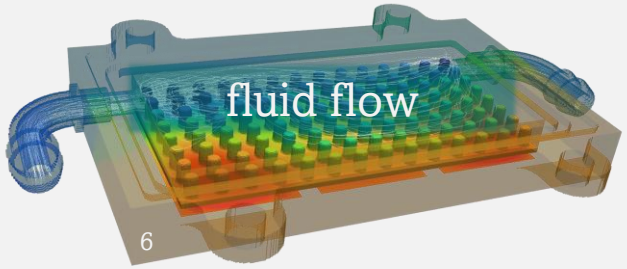

fluid flow

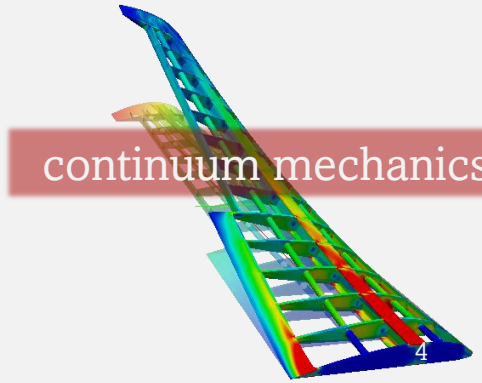

continuum mechanics

temperature

thermal expansion

1 SciTech Daily
2 Charged EVs
3 Talos VTOL
4 Simscale
5 COMSOL
6 Diabatix

Addressing the challenges

Phase change materials (**PCM**) are materials that store a considerable amount of thermal energy during the phase transition

The thermal storage capability of PCM makes it attractive for battery pack design to **regulate the temperature of batteries**

- ***PCM can absorb excess heat generated during charging or discharging, preventing overheating and extending the battery life***

Fan *et al.*, 2021

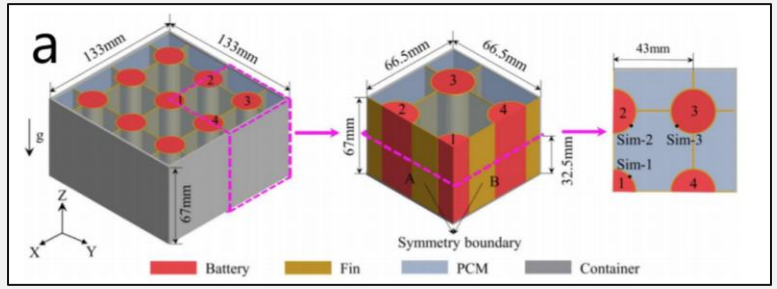

Choudhari *et al.*, 2021

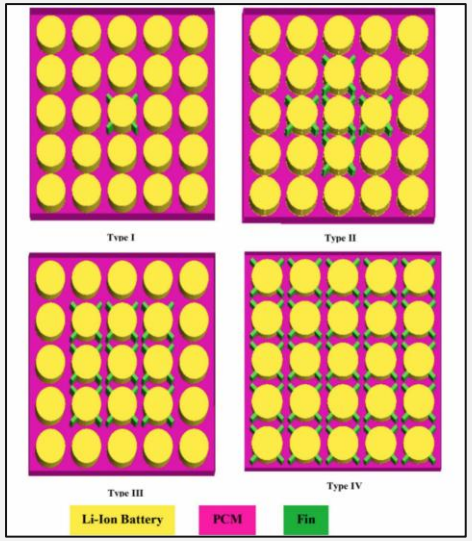

Liu *et al.*, 2021

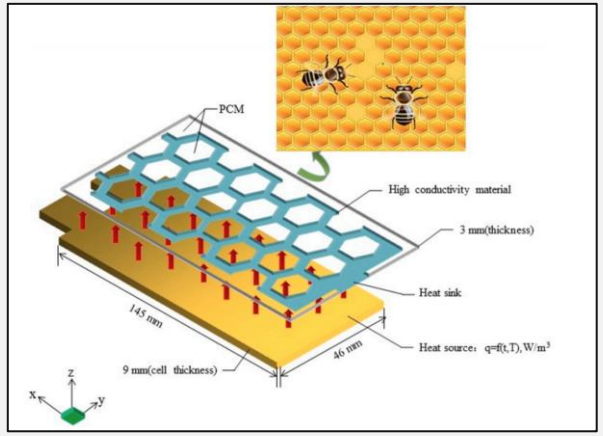

Traditional heat exchangers designs and biomimetic fins

1. Yu *et al.*, "*A review of battery thermal management systems about heat pipe and phase change materials*", Journal of Energy Storage 2023

Phase change materials

- Attractive the temperature of the batteries for **passive battery thermal management**
- PCM usually have low thermal conductivity → Incorporation of highly conductive materials (HCM) or heat pipes
- How to determine the distribution of HCM and PCM?
  Topology optimization

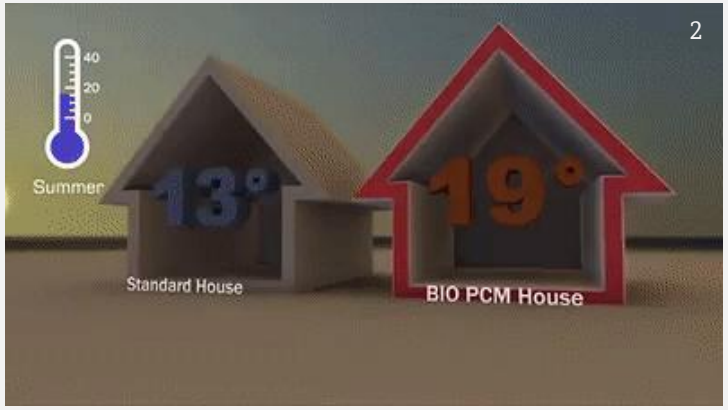

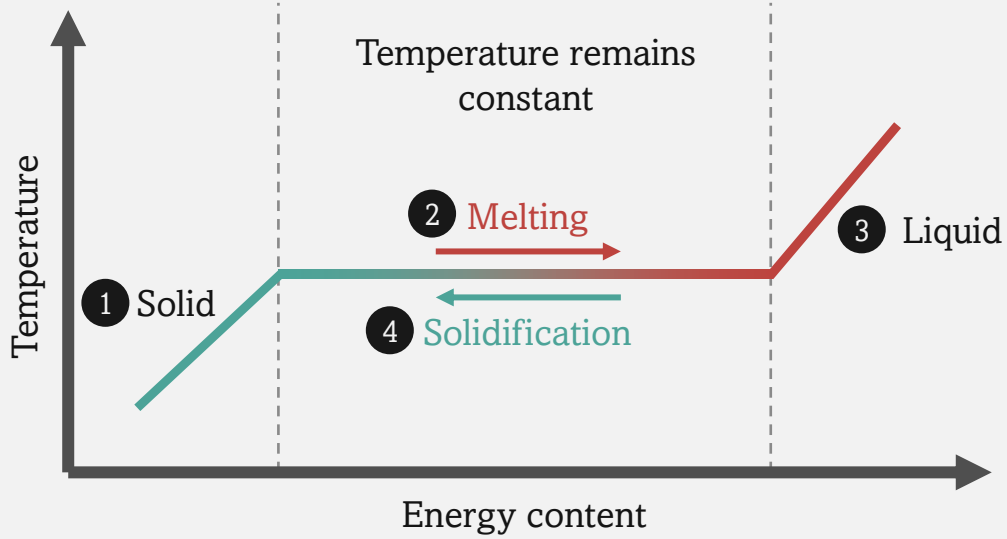

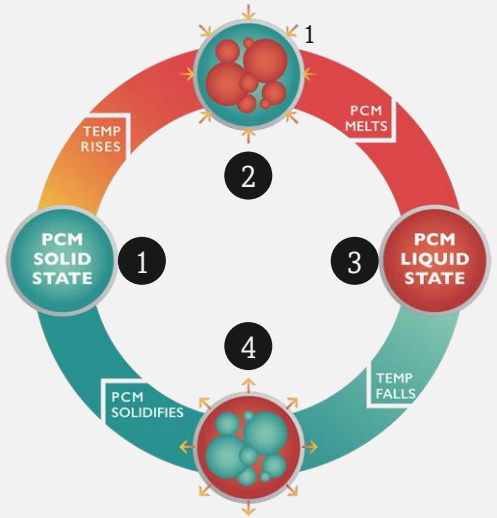

1. Zhan *et al.*, "*Phase change material (PCM) integrations into buildings in hot climates with simulation access for energy performance and thermal comfort: A review*", Construction and Building Materials 2023
2. Junhaokhoo

How to model PCM?

To account for the latent heat of fusion during phase change, the heat capacity is increased in the vicinity of the fusion temperature

- ***Apparent heat capacity method***

$$\tilde{c}_p(T) = \begin{cases} c_p \text{ for } T \in \left[0\,; T_f - \dfrac{\Delta T_f}{2}\right) \\ c_p + \dfrac{L_f}{\Delta T_f} \text{ for } T \in \left[T_f - \dfrac{\Delta T_f}{2}\,; T_f + \dfrac{\Delta T_f}{2}\right] \\ c_p \text{ for } T \in \left(T_f + \dfrac{\Delta T_f}{2}\,; T_{vap}\right) \end{cases}$$

$c_p = 1\,; L_f = 2\,; T_f = 0.5\,; \Delta T_f = 0.5$

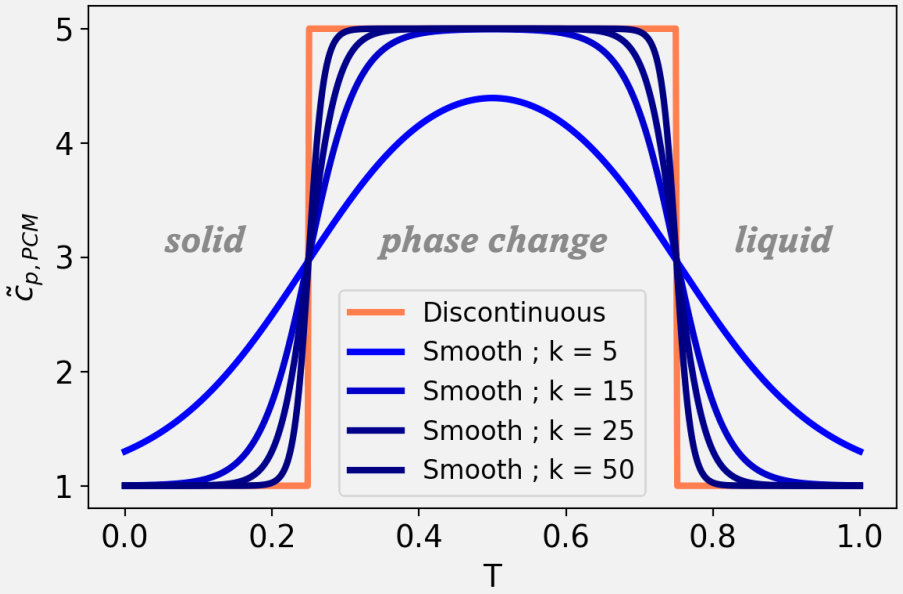

Approximated with a smooth function to be differentiable

$$\tilde{c}_p(T) \approx c_p^s + \frac{L_f}{\Delta T_f}\left(\frac{1}{1+e^{-2k(T-T_f+\Delta T_f/2)}} - \frac{1}{1+e^{-2k(T-T_f-\Delta T_f/2)}}\right)$$

Phase change is a transient process modeled with an unsteady heat diffusion model with temperature dependent heat capacity

$$\int_{\mathcal{D}} \rho \tilde{c}_p(T) v \frac{\partial T}{\partial t} dV + \int_{\mathcal{D}} \kappa \nabla_x v \cdot \nabla_x T dV = \int_{\mathcal{D}} vQ(t) dV - \int_{\Gamma_N} vq_n(t) dS - \int_{\Gamma_R} vh(T - T_{amb}) dS$$

Level-set topology optimization

Implicit description of the PCM domain over a structured grid using the level-set method

$$\begin{cases} \phi(\boldsymbol{x}) \geq 0 \Leftrightarrow \boldsymbol{x} \in \Omega_{\text{PCM}} \subseteq \mathcal{D} \\ \phi(\boldsymbol{x}) = 0 \Leftrightarrow \boldsymbol{x} \in \partial\Omega_{\text{PCM}} \\ \phi(\boldsymbol{x}) < 0 \Leftrightarrow \boldsymbol{x} \in \mathcal{D} \setminus \overline{\Omega_{\text{PCM}}} \end{cases}$$

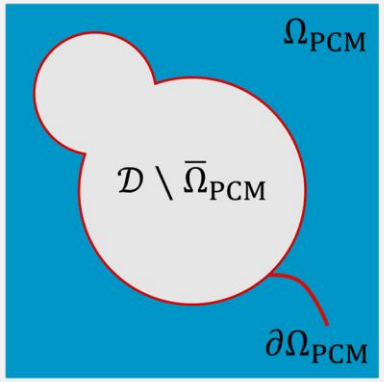

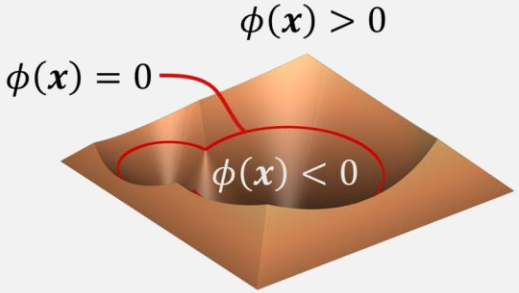

Boundaries updated at each optimization iteration via a **Hamilton-Jacobi equation**

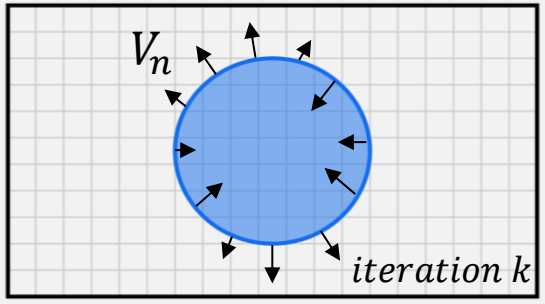

$$\frac{\mathrm{d}\phi}{\mathrm{dt}} + V_n|\nabla\phi| = 0 \quad \Rightarrow \quad \phi_j^{k+1} = \phi_j^k - \Delta t V_{n,j}|\nabla\phi_j^k|$$

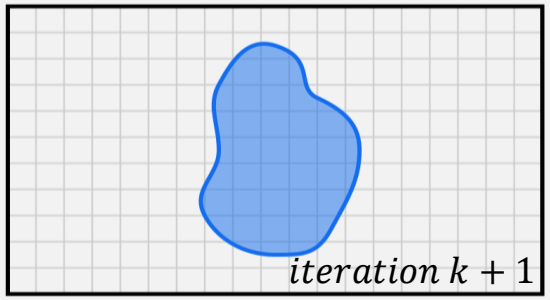

Dunning and Kim, "*Introducing the sequential linear programming level-set method for topology optimization*", SMO 2015

Material interpolation

Analysis on a structured grid

FEA using an Ersatz material approach with γ the fraction of the element with PCM

Linear interpolation of the material properties, e.g.,

$$\kappa_{\text{eff}} = \kappa_{\text{HCM}} + \gamma(\kappa_{\text{PCM}} - \kappa_{\text{HCM}})$$

Pros

- ✓ Simplified implementation: No need to explicitly track the PCM/HCM boundaries
- ✓ Computational efficiency: No remeshing during optimization
- ✓ Standard practice: Widely adopted in TO, including with PCM

Cons

- ❑ Approximation at interfaces: PCM/HCM boundaries are only approximated

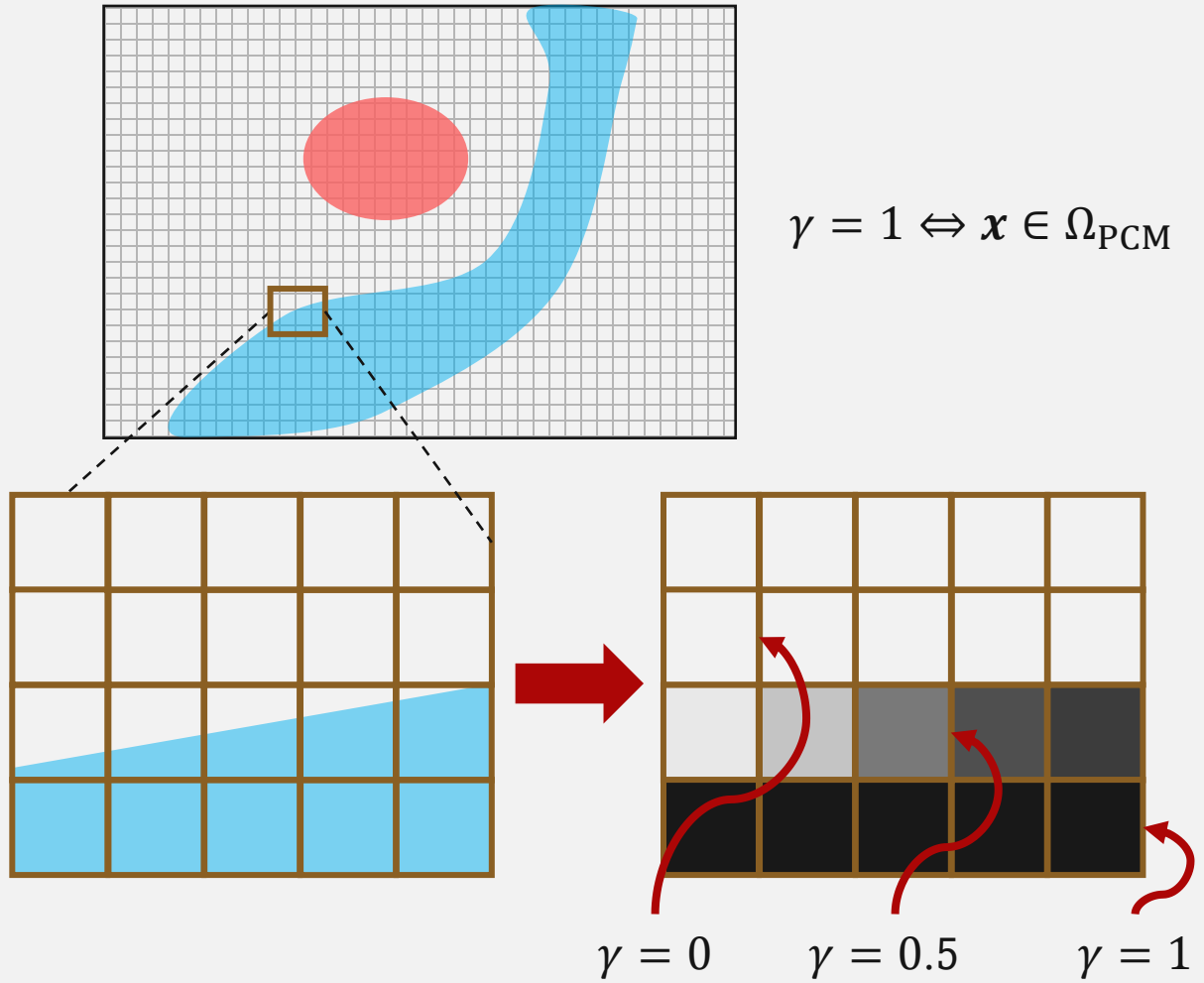

Level-set topology optimization with PCM

We want to design a heat sink that **minimize the temperature oscillations**

Large temperature variations lead to faster degradation of batteries and fatigue-induced failure due to mismatch of the coefficients of thermal expansion

- Spatial averaging → $\langle T \rangle \triangleq \frac{\int_{\mathcal{D}} T dV}{\int_{\mathcal{D}} 1 dV}$
- Temporal averaging → $\langle \bar{T} \rangle \triangleq \frac{\sum_{i=0}^{N} \langle T \rangle^i}{N}$
- Temporal variance → $\mathbb{V}(\langle T \rangle) \triangleq \frac{\sum_{i=0}^{N} (\langle T \rangle^i - \langle \bar{T} \rangle)^2}{N}$

minimize	$J \triangleq \mathbb{V}(\langle T \rangle)$
subject to	$V \leq \xi V_0$

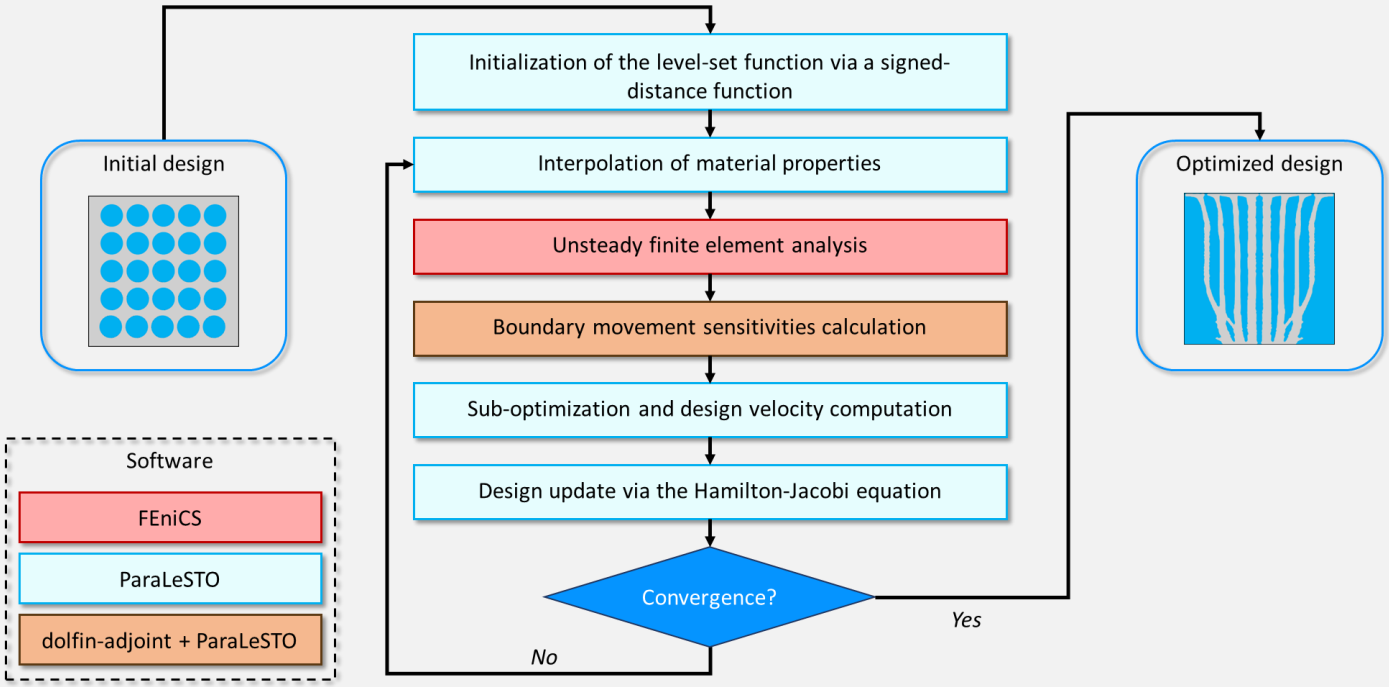

Temperature oscillations minimization with heat flux heat source

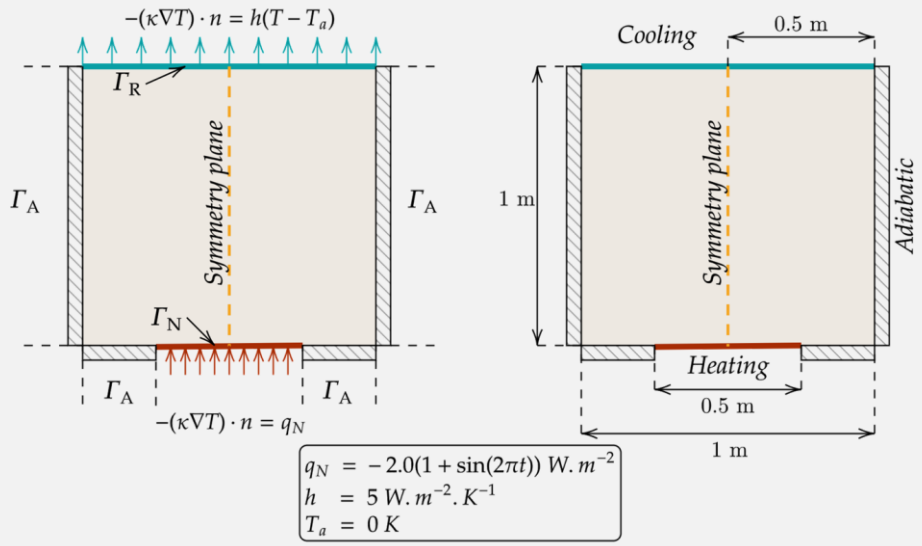

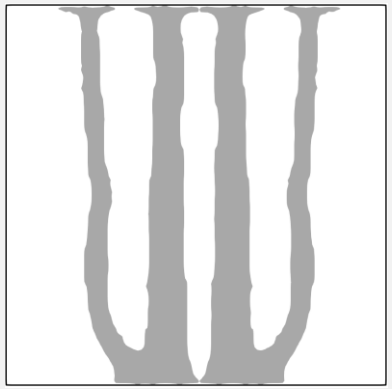

HCM only

$\xi = 0.3$

HCM+PCM

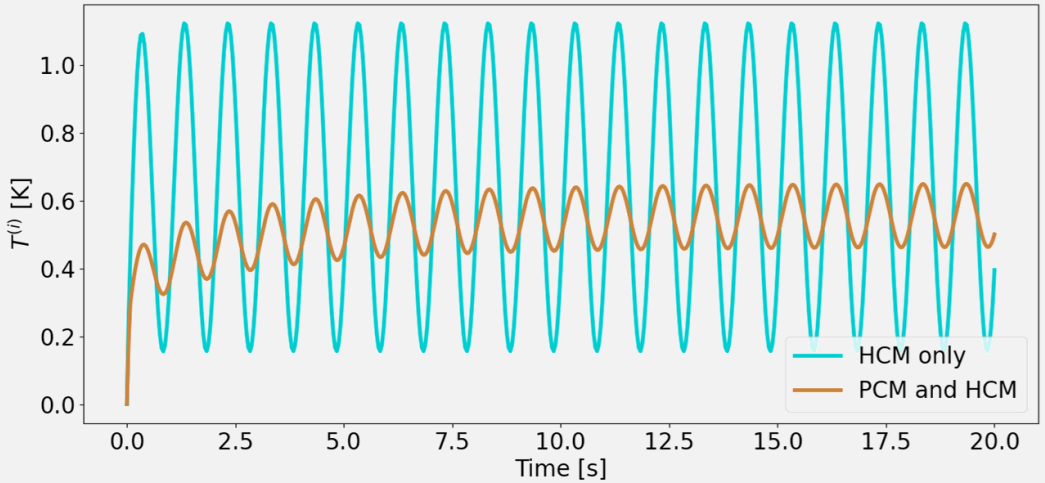

Variance reduction: 94%
Max. reduction: 42%
Mean reduction: 18%

Temperature oscillations minimization with heat flux heat source

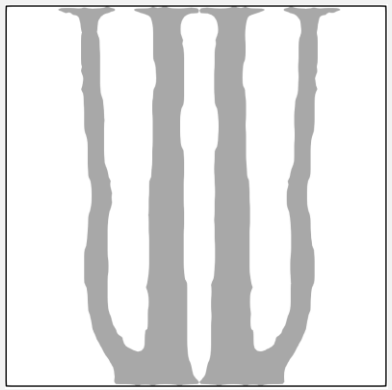

HCM only

HCM+PCM

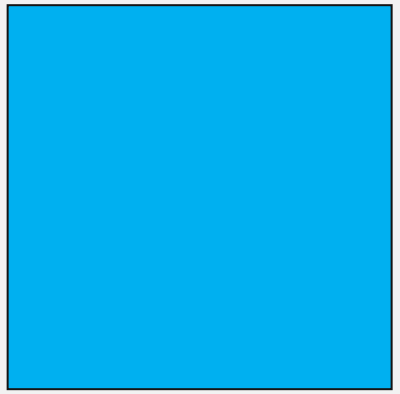

100% PCM

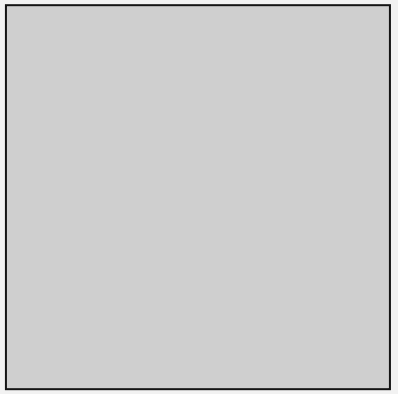

100% HCM

Case	Quantity of Interest	Value
Optimized for PCM and HCM	Maximum temperature [K]	0.649
	Mean temperature [K]	0.525
	Temporal variance J [K^2]	0.0067
Optimized for HCM only	Maximum temperature [K]	1.122
	Mean temperature [K]	0.637
	Temporal variance J [K^2]	0.1176
100% HCM ; $\xi = 1.0$	Maximum temperature [K]	0.471
	Mean temperature [K]	0.300
	Temporal variance J [K^2]	0.0144
100% PCM ; $\xi = 0.0$	Maximum temperature [K]	18,879.3
	Mean temperature [K]	9,970.3
	Temporal variance J [K^2]	39,774,330.5

Only PCM results in **insulating effects**

HCM, as expected, lower max. and mean temperature but **114% higher variance than with the inclusion of PCM**

Updated workflow to consider the batteries

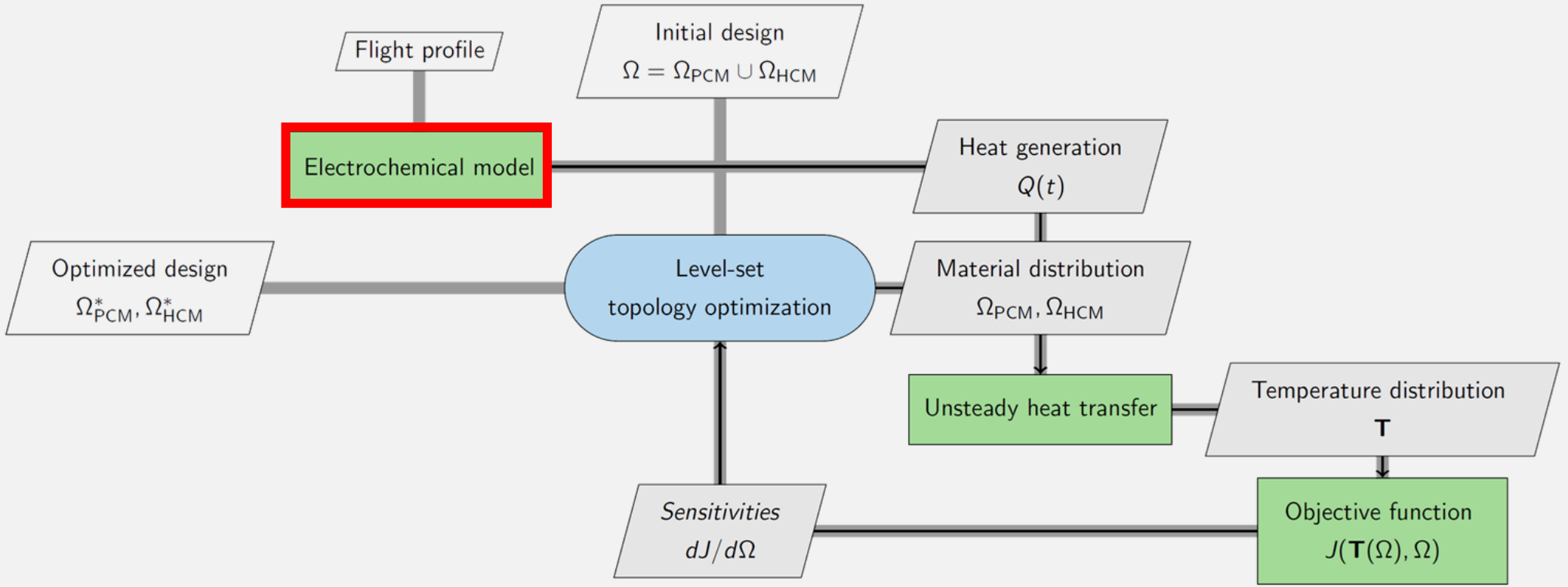

Battery model

PyBaMM

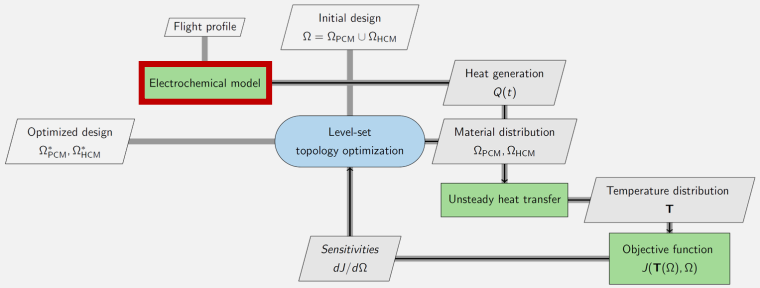

Doyle Fuller Newman (DFN) model

Physics-based battery models

- Charge conservation
- Mass conservation
- Electrochemical reactions

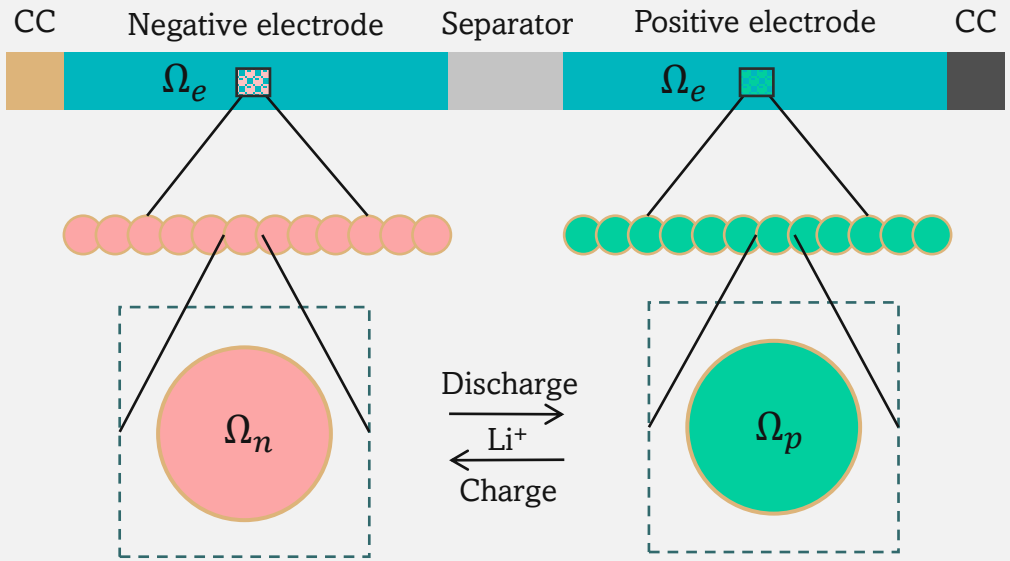

Negative electrode

$$\nabla \cdot i_n = -j_k$$

$$\frac{\partial c_n}{\partial t} + \nabla \cdot N_n = 0$$

Positive electrode

$$\nabla \cdot i_p = -j_k$$

$$\frac{\partial c_p}{\partial t} + \nabla \cdot N_p = 0$$

Interface

$$j_k = j_{k0}(c_e, c_k) \sinh\left(\frac{F}{2RT}\eta(\phi_e, \phi_k)\right)$$

$$k \in \{n, p\}$$

Electrolyte

$$\nabla \cdot i_e = j_k$$

$$\frac{\partial c_e}{\partial t} + \nabla \cdot N_e = \frac{j_k}{F}$$

Guibert *et al.*, "*Thermo-electrochemical level-set topology optimization of a heat exchanger for LiB for eVTOL vehicles*", Appl. Therm. Eng. 2024

Heat transfer model

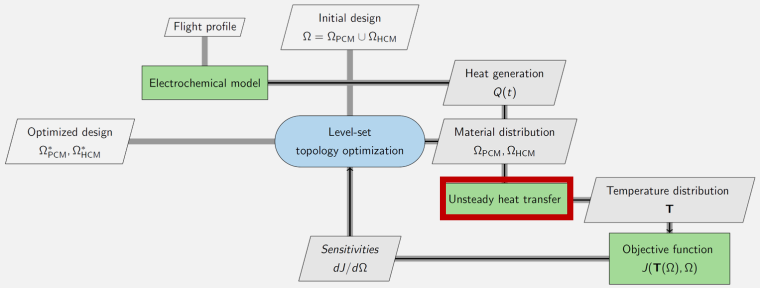

The governing equation for unsteady heat transfer is

$$\nabla \cdot (\kappa \nabla T) + Q(t) = \rho c_p \frac{\partial T}{\partial t}$$

$Q(t)$: volumetric heat generation from the electrochemical model

Time derivative → unconditionally stable backward Euler scheme

$$\frac{\partial T^{(i)}}{\partial t} \approx \frac{T^{(i)} - T^{(i-1)}}{\Delta t}$$

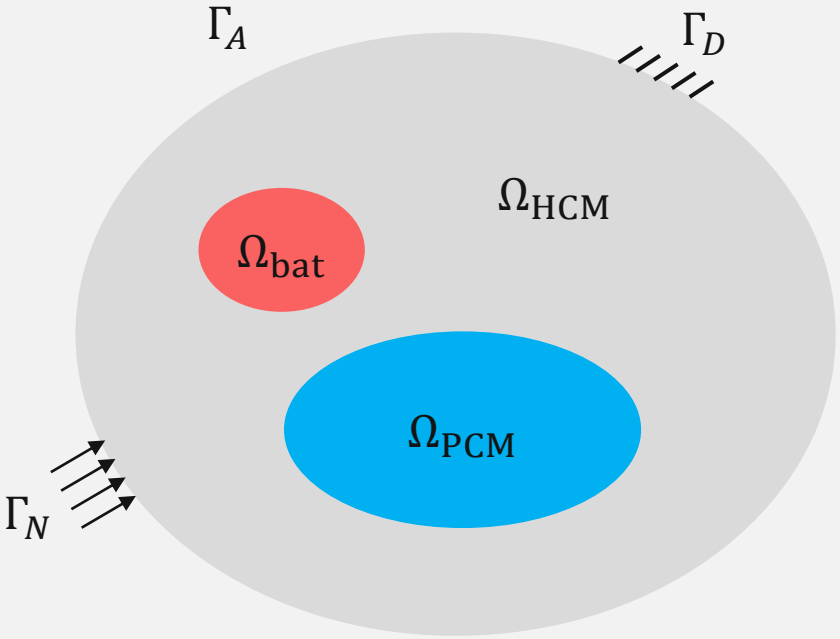

$$\mathcal{D} = \Omega_{bat} \cup \Omega_{PCM} \cup \Omega_{HCM}$$

$$\partial\mathcal{D} = \Gamma_D \cup \Gamma_N \cup \Gamma_A$$

Optimization problem

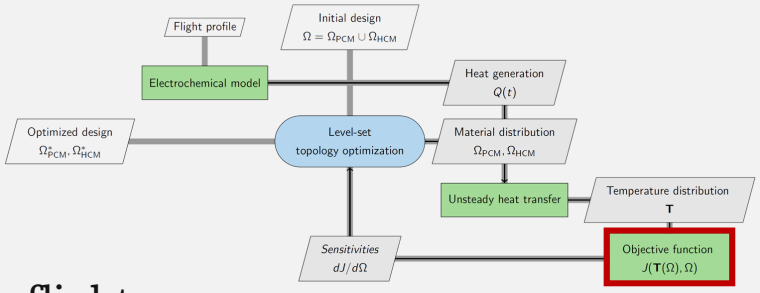

The objective is to minimize the temperature variance in the batteries during the flight.

The **spatially averaged** temperature increase in the batteries at time step i is

$$\bar{T}^{(i)} \triangleq \frac{1}{N_n} \sum_{n \in \Omega_{\text{bat}}} T_n^{(i)}$$

The temperature **temporal variance** in the batteries is defined as

$$\mathbb{V}(\langle \bar{T} \rangle) \triangleq \frac{1}{N_t} \sum_{i=0}^{N_t} \left(\bar{T}^{(i)} - \langle \bar{T} \rangle \right)^2 \text{ where } \quad \langle \bar{T} \rangle \triangleq \frac{1}{N_t} \sum_{i=0}^{N_t} \bar{T}^{(i)}$$

The optimization problem $\mathcal{O}_1$ reads

$$\mathcal{O}_1 \begin{cases} \min & \mathcal{F} = \mathbb{V}(\langle \bar{T} \rangle) \\ \text{subject to} & \text{Vol}(\Omega_{\text{HCM}}) \leq 0.5 \, \text{Vol}(\mathcal{D}) \end{cases}$$

Numerical examples

LG M50 21700
Lithium-ion battery

Commercially available with high-energy density
$\approx 260\ \mathrm{Wh.\,kg^{-1}}$

Segment	Short takeoff/landing (ST/L)	Long takeoff/landing (LT/L)
Takeoff	30 s at 3 C (15 A/cell)	150 s at 1.5 C (7.5 A/cell)
Cruise	300 s at 1 C (5 A/cell)	300 s at 1 C (5 A/cell)
Landing	30 s at 3 C (15 A/cell)	150 s at 1.5 C (7.5 A/cell)

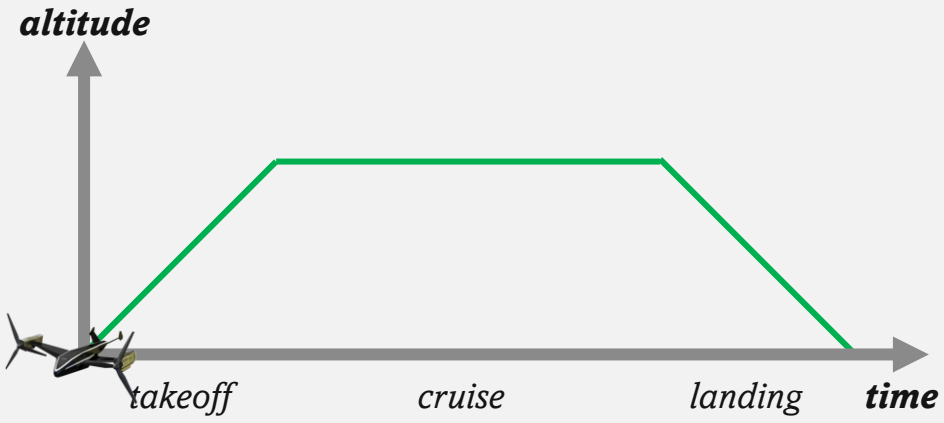

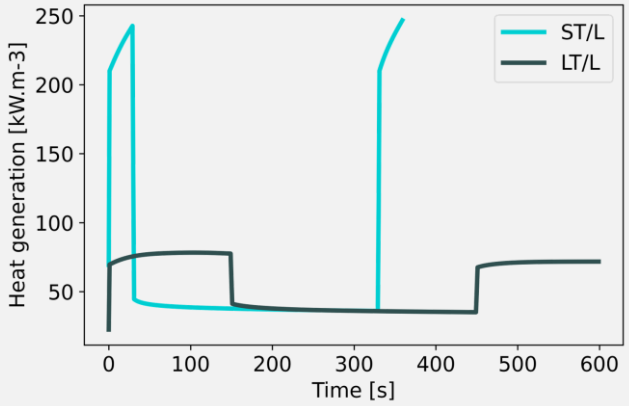

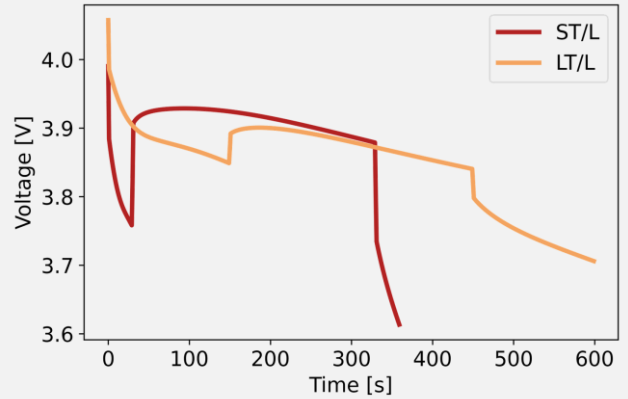

Numerical examples

Property	PCM[1] Paraffin wax	HCM Aluminum	Batteries[2,3] LG M50 LiB
Conductivity $[\mathrm{W.m^{-1}.K^{-1}}]$	0.2	237	23
Mass density $[\mathrm{kg.m^{-3}}]$	880	2700	2805
Heat capacity $[\mathrm{J.kg^{-1}.K^{-1}}]$	1800	903	630
Temperature of fusion [K]	308	-	-
Latent heat of fusion $[\mathrm{kJ.kg^{-1}}]$	157	-	-
Melting temperature range [K]	5	-	-

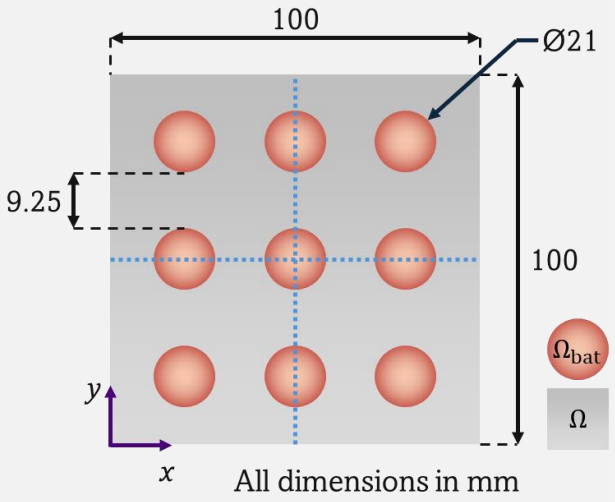

$Q(t)$: volumetric heat generation

$-\kappa\nabla T \cdot \boldsymbol{n} = h(T - T_{amb})$: natural convection

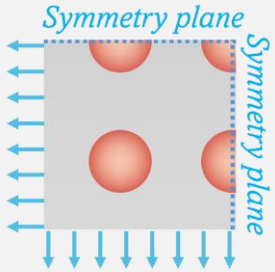

100 x 100

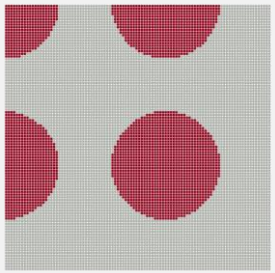

→ $\approx 0.1 - 0.2$ s per timestep

1. Laasri *et al.*, "*Investigation of different topology-optimized fin structures in a cylindrical latent heat thermal energy storage unit,*", Therm. Sci. Eng. Prog. 2022
2. Guibert *et al.*, *"Thermo-electrochemical level-set topology optimization of a heat exchanger for lithium-ion batteries for electric vertical take-off and landing vehicles"*, Appl. Therm. Eng. 2024
3. Chen *et al.*, *"Development of experimental techniques for parameterization of multi-scale lithium-ion battery models"*, JES 2020

Results

ST/L

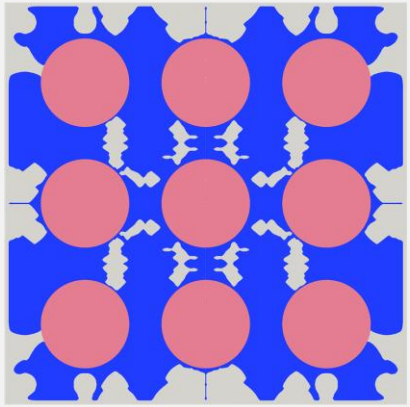

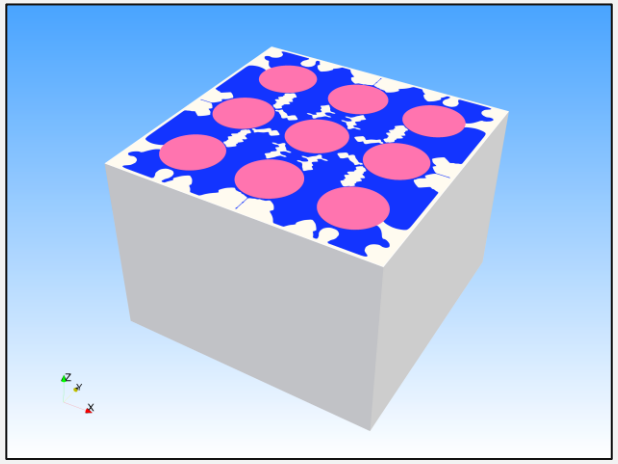

LT\L

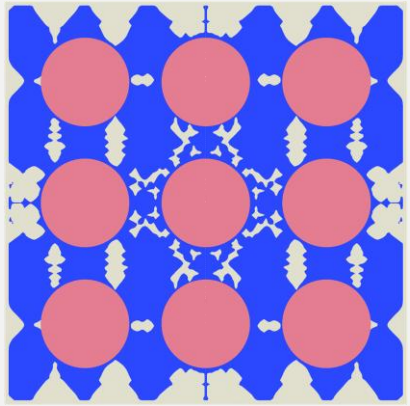

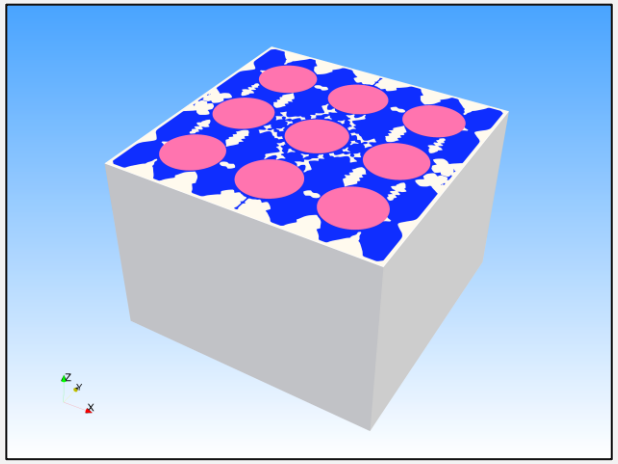

PCM HCM Batt.

ΔT_{max} [K]

Configuration	ST/L	LT/L
TO PCM/HCM	4.26	3.96
PCM only	5.03	4.75
HCM only	3.45	4.18

$\mathcal{F}$ [K^2]

Configuration	ST/L	LT/L
TO PCM/HCM	0.390	0.697
PCM only	0.608	1.041
HCM only	0.432	1.127

Temperature variance change ($\mathcal{F}$)

ST/L: **-36%** PCM only | **-10%** HCM only

LT/L: **-33%** PCM only | **-38%** HCM only

PCM with active cooling

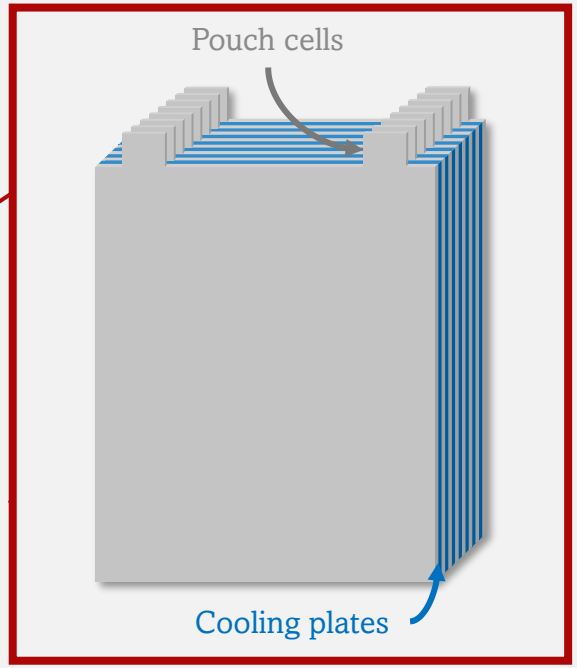

- ***We can use topology optimization to design non-conventional cooling plates that embed phase-change materials (PCM)***

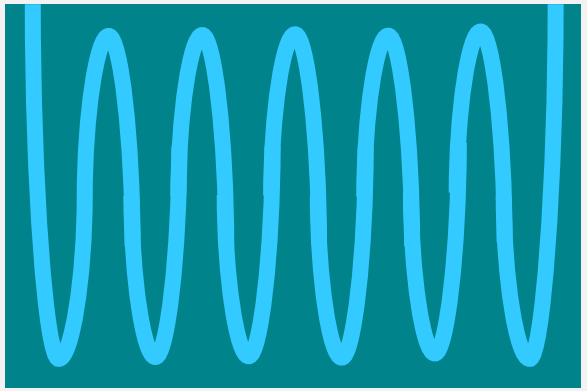

Topology optimized cooling plates with **phase change materials**

Workflow

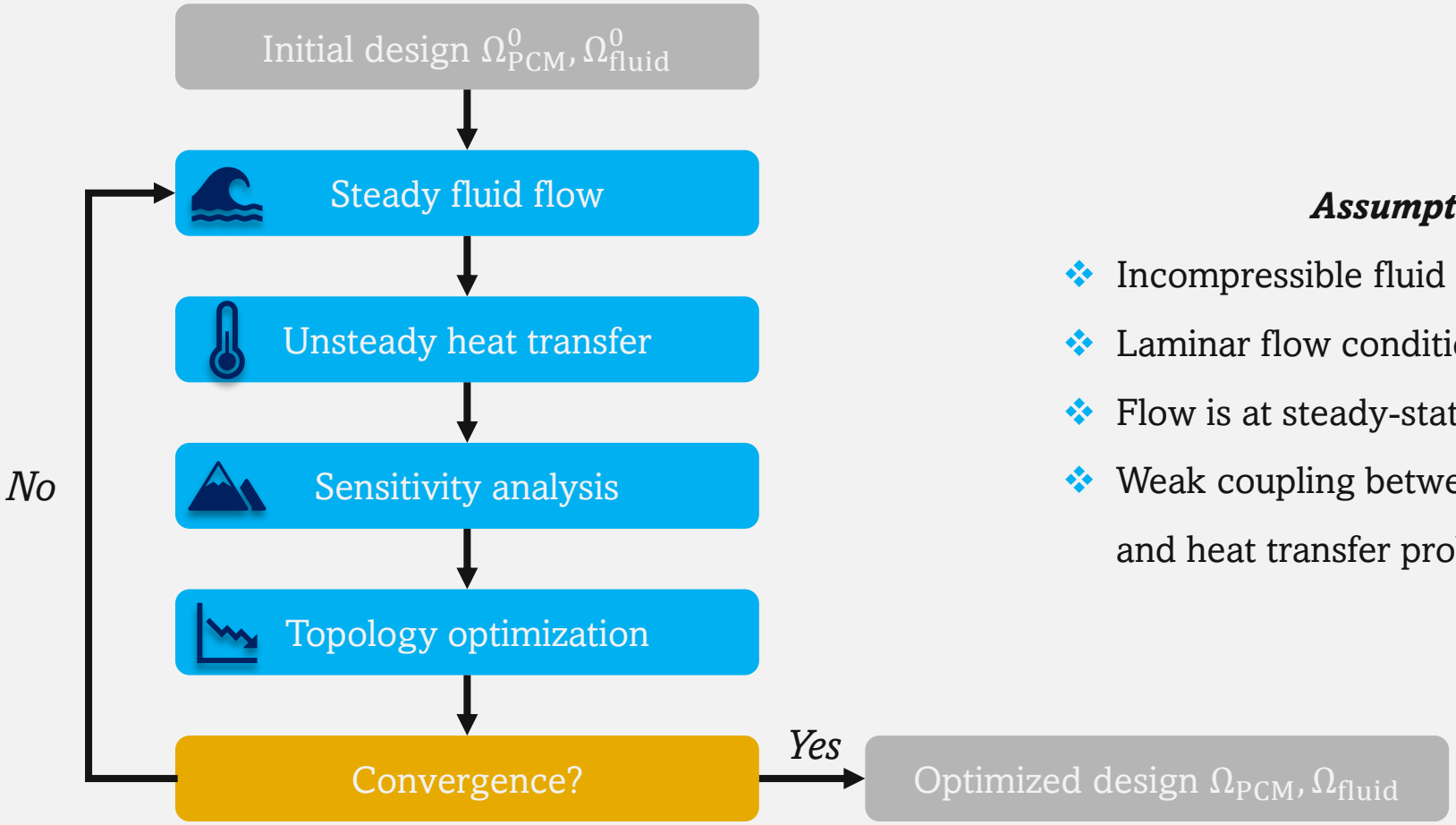

Assumptions

- Incompressible fluid
- Laminar flow conditions
- Flow is at steady-state
- Weak coupling between the fluid flow and heat transfer problems

Conjugate heat transfer

Navier-Stokes with Brinkman penalization

$$\rho(\boldsymbol{u}\cdot\nabla\boldsymbol{u}) - \mu\nabla^2\boldsymbol{u} + \nabla p + \alpha\boldsymbol{u} = \boldsymbol{0}$$
$$\nabla\cdot\boldsymbol{u} = 0$$

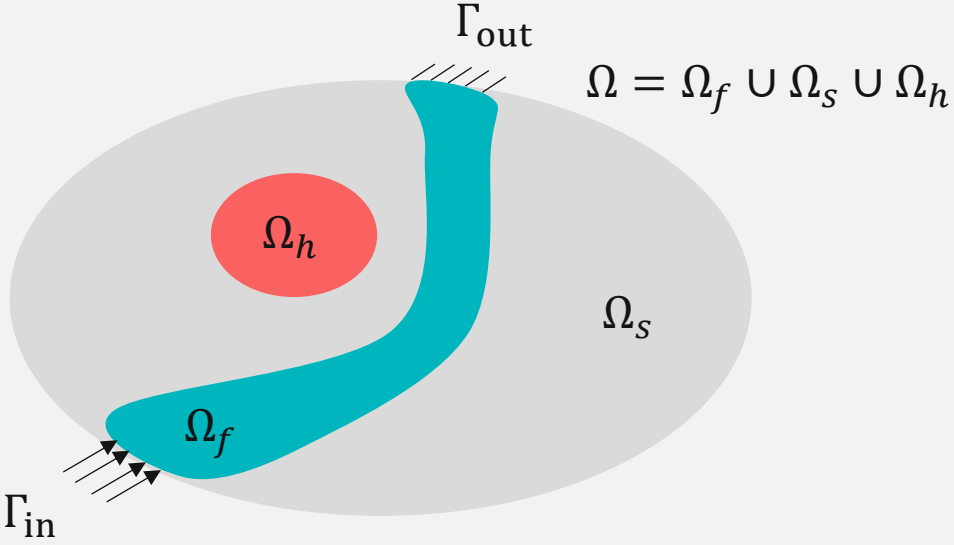

Transient convection-diffusion equation

$$\rho c_p(T)\boldsymbol{u}\cdot\nabla T + \rho c_p(T)\frac{\partial T}{\partial t} - k\nabla^2 T - Q = 0$$

convective term

storage term (*implicit Euler*)

diffusive term

heat source (e.g., from electronics)

$$\boldsymbol{u}\cdot\boldsymbol{n} = \boldsymbol{u_{in}} \text{ on } \Gamma_{\text{in}} \qquad T = T_{\text{in}} \text{ on } \Gamma_{\text{in}}$$
$$Q = Q_0 \text{ in } \Omega_h \qquad p = p_{\text{out}} \text{ on } \Gamma_{\text{out}}$$
$$\boldsymbol{u}\cdot\boldsymbol{n} = \boldsymbol{0} \text{ on } \partial\Omega \setminus (\Gamma_{\text{in}} \cup \Gamma_{\text{out}})$$
$$\frac{\partial T}{\partial \boldsymbol{n}} = 0 \text{ on } \partial\Omega \setminus \Gamma_{\text{in}}$$

Problem definition

Minimize pressure drop subject to an upper bound on the cooling plate's average temperature.

- ***Pressure drop*** (reduces pumping power)

$$P_d := \frac{1}{l_{\text{in}}} \int_{\Gamma_{\text{in}}} p \, \text{ds} - \frac{1}{l_{\text{out}}} \int_{\Gamma_{\text{out}}} p \, \text{ds}$$

- ***Spatially averaged temperature at the last time step*** (promotes better cooling)

$$\bar{T} := \frac{1}{A} \int_{\Omega} T^{(N_t)} \, \text{dv}$$

The optimization problem $\mathcal{O}_1$ reads

$$\mathcal{O}_1 \begin{cases} \min\limits_{\phi} & P_d \\ \text{subject to} & \bar{T} \leq \bar{T}_0 \end{cases}$$

Sensitivity analysis

The design sensitivities are computed using the discrete adjoint method

$$\mathcal{L} = \mathcal{F} + \boldsymbol{\lambda}_{NS} \cdot \boldsymbol{R}_{NS} + \sum_{i=1}^{N_t} \boldsymbol{\lambda}_{\boldsymbol{T}}^{(i)} \cdot \boldsymbol{R}_{\boldsymbol{T}}^{(i)}$$

With $N_t + 1$ adjoint equations and $\boldsymbol{X} \coloneqq [\boldsymbol{u}^h \; \boldsymbol{p}^h]^\mathsf{T}$ such that

$$\begin{cases} \left(\dfrac{\partial \boldsymbol{R}_{\boldsymbol{T}}^{(\mathrm{N_t})}}{\partial \boldsymbol{T}^{(N_t)}}\right)^\mathsf{T} \boldsymbol{\lambda}_{\boldsymbol{T}}^{(N_t)} = -\dfrac{\partial \mathcal{F}}{\partial \boldsymbol{T}^{(N_t)}} \\ \left(\dfrac{\partial \boldsymbol{R}_{\boldsymbol{T}}^{(i)}}{\partial \boldsymbol{T}^{(i)}}\right)^\mathsf{T} \boldsymbol{\lambda}_{\boldsymbol{T}}^{(i)} = -\dfrac{\partial \mathcal{F}}{\partial \boldsymbol{T}^{(i)}} - \left(\dfrac{\partial \boldsymbol{R}_{\boldsymbol{T}}^{(i+1)}}{\partial \boldsymbol{T}^{(i)}}\right)^\mathsf{T} \boldsymbol{\lambda}_{\boldsymbol{T}}^{(i+1)} \quad \forall i = N_t - 1, \dots, 1 \\ \left(\dfrac{\partial \boldsymbol{R}_{\boldsymbol{NS}}^{(1)}}{\partial \boldsymbol{X}}\right)^\mathsf{T} \boldsymbol{\lambda}_{\boldsymbol{NS}} = -\dfrac{\partial \mathcal{F}}{\partial \boldsymbol{X}} - \sum_{i=1}^{N_t} \left(\dfrac{\partial \boldsymbol{R}_{\boldsymbol{T}}^{(i)}}{\partial \boldsymbol{X}}\right)^\mathsf{T} \boldsymbol{\lambda}_{\boldsymbol{T}}^{(i)} \end{cases}$$

Finally, the total derivative is expressed as

$$\frac{d\mathcal{F}}{d\boldsymbol{\gamma}} = \frac{\partial \mathcal{F}}{\partial \boldsymbol{\gamma}} + \left(\frac{\partial \boldsymbol{R}_{\boldsymbol{NS}}}{\partial \boldsymbol{\gamma}}\right)^\mathsf{T} \boldsymbol{\lambda}_{\boldsymbol{NS}} + \sum_{i=1}^{N_t} \left(\frac{\partial \boldsymbol{R}_{\boldsymbol{T}}^{(i)}}{\partial \boldsymbol{\gamma}}\right)^\mathsf{T} \boldsymbol{\lambda}_{\boldsymbol{T}}^{(i)}$$

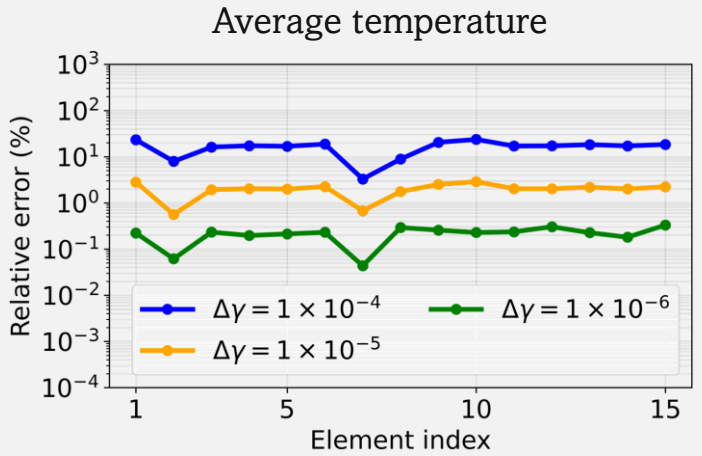

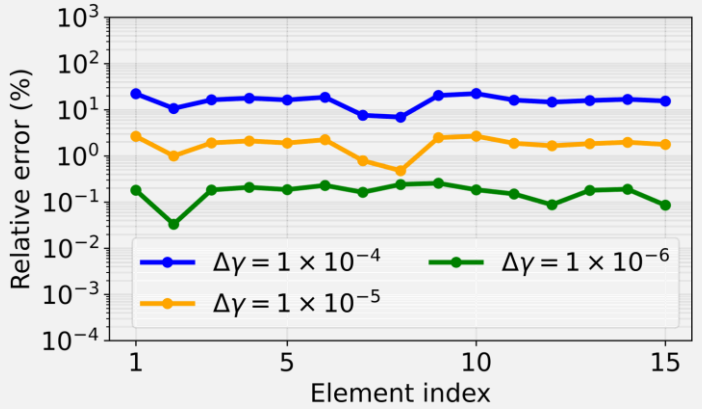

Validation against finite differences for 15 randomly selected elements

$$\frac{d\mathcal{F}(\gamma_i)}{d\gamma_i} \approx \frac{\mathcal{F}(\gamma_i) - \mathcal{F}(\gamma_i - \Delta\gamma)}{\Delta\gamma}$$

Numerical experiments

Property	PCM	Fluid
Conductivity [$\mathrm{W.m^{-1}.K^{-1}}$]	5.0×10^{-2}	1.0×10^{0}
Mass density [$\mathrm{kg.m^{-3}}$]	1.0×10^{0}	1.0×10^{0}
Dynamic viscosity [Pa. s]	-	1.0×10^{-2}
Heat capacity [$\mathrm{J.kg^{-1}.K^{-1}}$]	2.0×10^{1}	5.0×10^{0}
Temperature of fusion [K]	5.0×10^{0}	-
Latent heat of fusion [$\mathrm{J.kg^{-1}}$]	4.0×10^{1}	-
Melting temperature range [K]	5.0×10^{-1}	

Reynolds number ($\rho u_{in} l_{in}/\mu$) *Ratio of inertial forces to viscous forces*	1.0×10^{2}
Péclet number ($\rho c_p u_{in} l_{in}/\kappa$) *Ratio of rate of advection to rate of diffusion*	5.0×10^{0}
Discretization	120×80

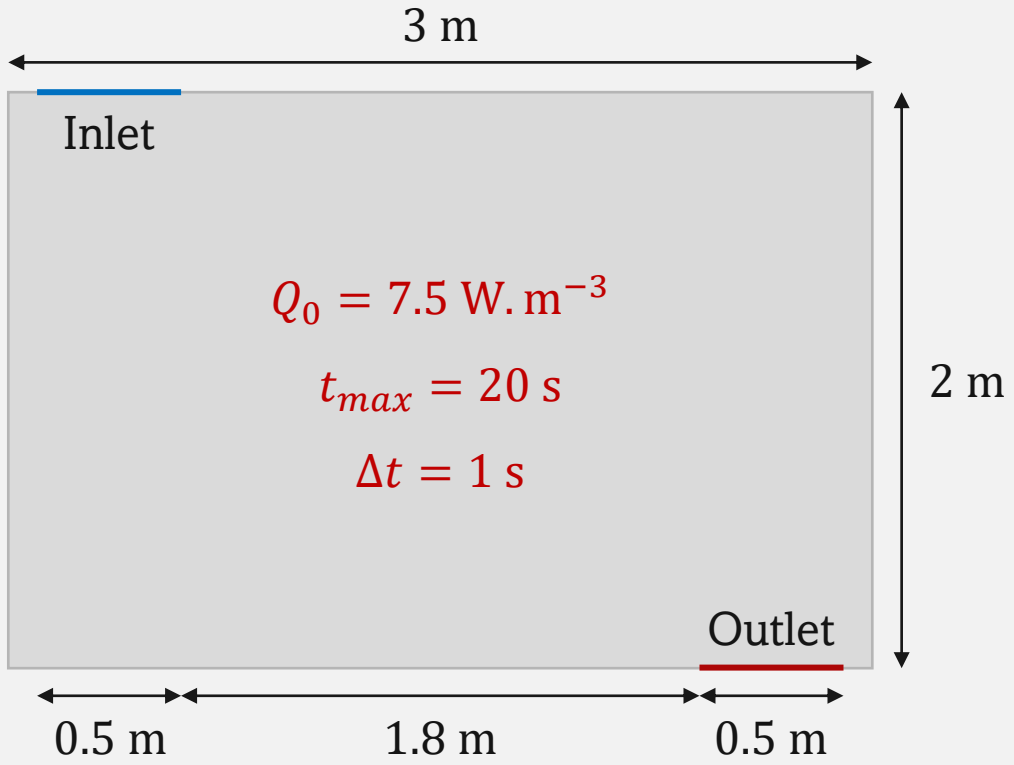

Parabolic inlet velocity profile

$u_{\mathrm{in,max}} = 2.0\ \mathrm{m.s^{-1}}$

Influence of temperature constraint

$$\mathcal{O}_1 \begin{cases} \min\limits_{\phi} & P_d \\ \text{subject to} & \bar{T} \leq \bar{T}_0 \end{cases}$$

$\bar{T}_0$ [K]	P_d [Pa]
5.00	7.71
5.25	4.38
5.50	3.26
5.75	2.58

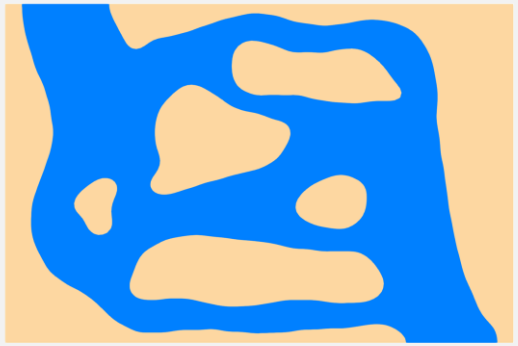

$\bar{T}_0 = 5.00$

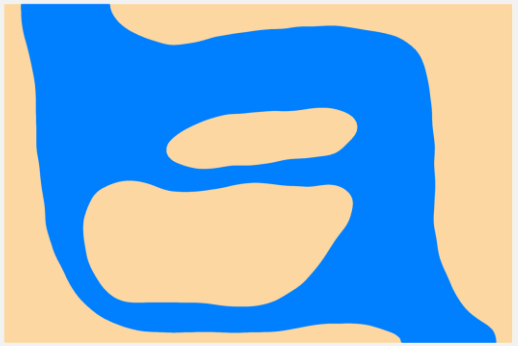

$\bar{T}_0 = 5.25$

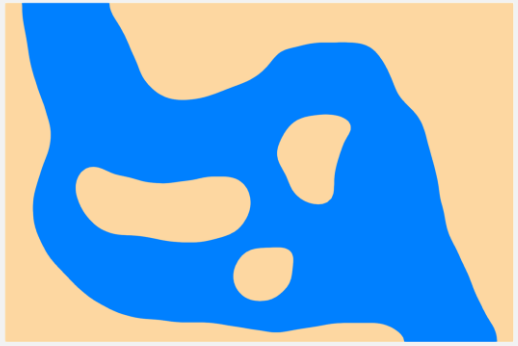

$\bar{T}_0 = 5.50$

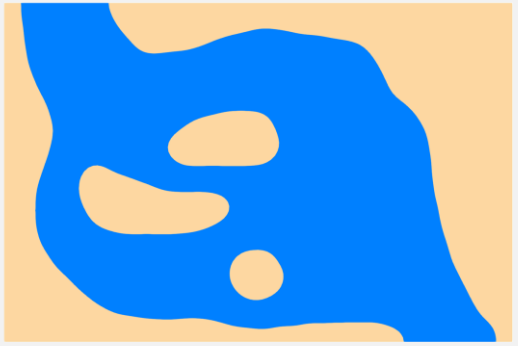

$\bar{T}_0 = 5.75$

As $\bar{T}_0$ is relaxed, the flow path evolves from a densely branched network to larger channels

→ **trade-off between PCM contact area and pressure drop**

Influence of latent heat of fusion

$$\mathcal{O}_1 \begin{cases} \min\limits_{\phi} & P_d \\ \text{subject to} & \bar{T} \leq 5 \end{cases}$$

$L_f = 40$

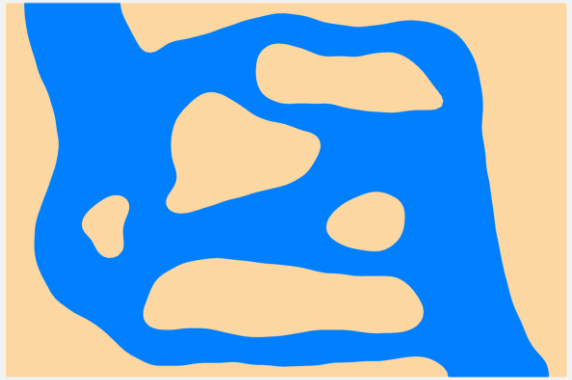

$L_f = 60$

$L_f = 80$

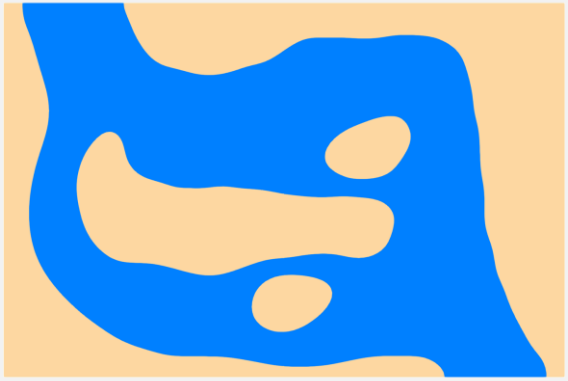

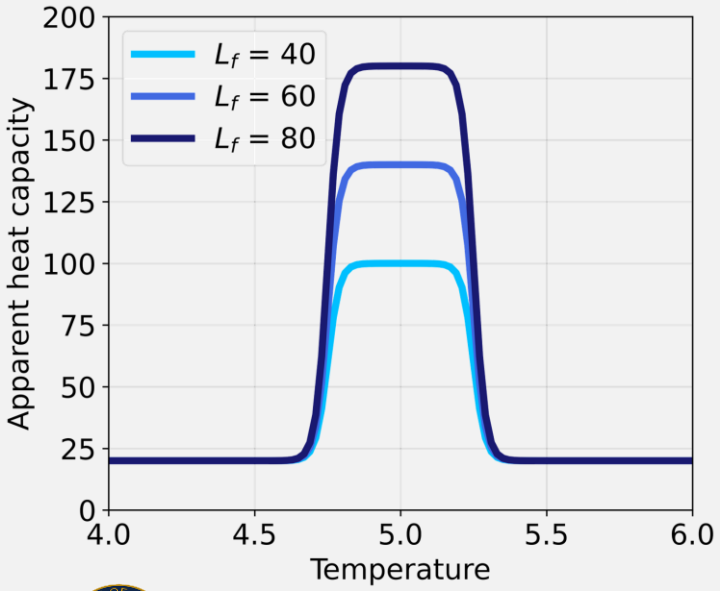

Latent heat of fusion $[\mathrm{J.kg^{-1}}]$	P_d [Pa]
40	7.71
60	7.02
80	4.12

As L_f increases, the topology simplifies with **less PCM inclusions** reflecting lower PCM/fluid surfaces needed and yielding **lower pressure drop**

Influence of latent heat of fusion

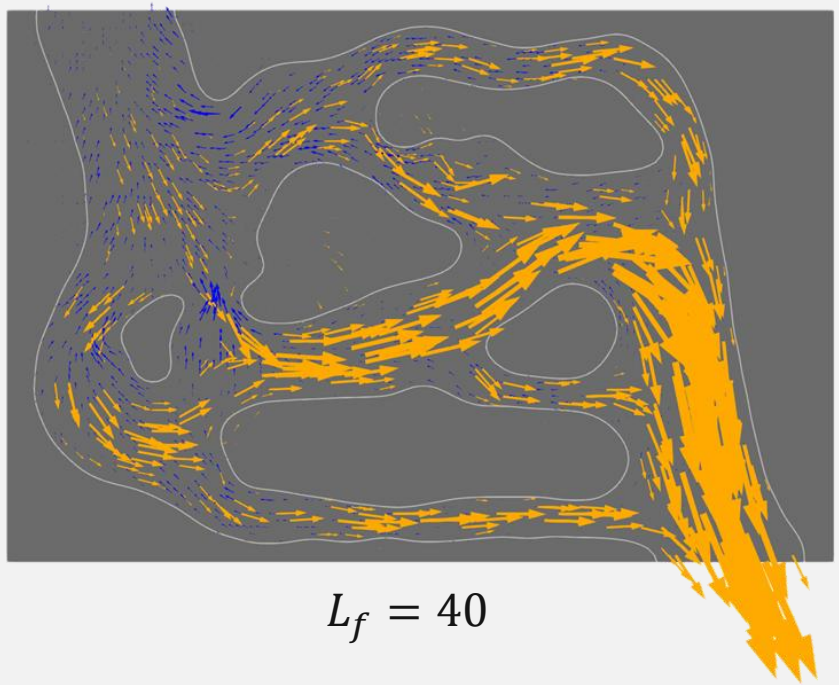

$L_f = 40$

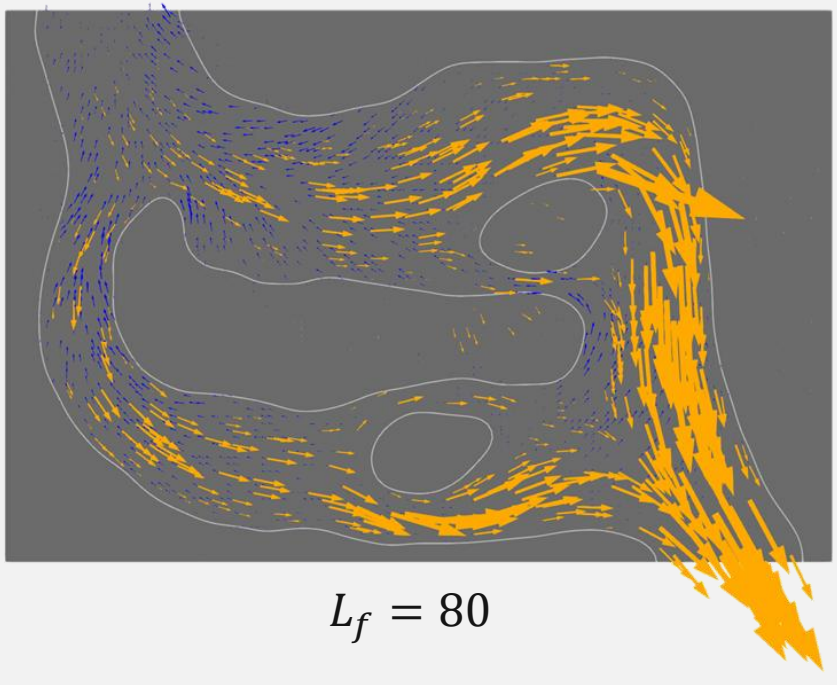

$L_f = 80$

Convective heat flux in orange

$$q_{\text{conv}} = \rho c_p T \boldsymbol{u}$$

Conductive heat flux

$$q_{\text{cond}} = -k\nabla \text{T}$$

Channel advection dominates

Convective term in the fluid far exceeds conduction in the domain

PCM storage

Conduction is the only mechanism in PCM with lower heat flux highlighting its role for energy storage rather than as a rapid transport medium

Conclusions

Work completed

✓ Developed level-set topology optimization for unsteady heat transfer with PCM including conjugate heat transfer for battery packs

Future directions

- ❑ Further investigate the relationship between heat generation profiles and optimized designs
- ❑ Look into other optimization formulations (e.g., maximum temperature, spatial/temporal variance)
- ❑ Investigate additional thermal loading conditions

Acknowledgments

This work was supported by a NASA ULI project (award No. 80NSSC21M0070), LG Energy Solution through the Frontier Research Laboratory (FRL) program, and Honda Performance Development (Project 2021249.1.896934)

References

1. A. Guibert, *et al.*, "*Thermo-electrochemical level-set topology optimization of a heat exchanger for lithium-ion batteries for eVTOL*", Applied Thermal Engineering (2024)
2. A. Guibert, *et al.*, "*Level-set topology optimization of heat sinks with phase-change material*", International Journal of Heat and Mass Transfer (2024)
3. A. Guibert, *et al.*, "*Thermal-Fluid-Electrochemical Topology Optimization of Lithium-Ion Cooling Plates via a Level-Set Approach*", Journal of Energy Storage (2025)
4. J. Kim, *et al.*, "*Design parameter optimization for sulfide-based all-solid-state batteries with high energy density*", eTransportation (2025)
5. A. Guibert, *et al.*, "*Thermo-mechanical level-set topology optimization of a load carrying battery pack for electric aircraft*", ECCOMAS (2023)
6. A. Guibert, *et al.*, "*Multifidelity Uncertainty Quantification in Battery Performance for eVTOL Flights Under Material and Loading Uncertainties*", VFS Forum (2024)
7. A. Guibert, *et al.*, "*Thermo-Mechanical Level-Set Topology Optimization of an eVTOL Battery Pack*", SciTech (2024)
8. A. Guibert, *et al.*, "*Design of electric aircraft battery packs embedded with phase-change material via level-set topology optimization*", SciTech (2025)
9. M. Bookwala, *et al.*, "*Shape Optimization of Porous Electrode Batteries*", SciTech (2025)

Influence of temperature constraint

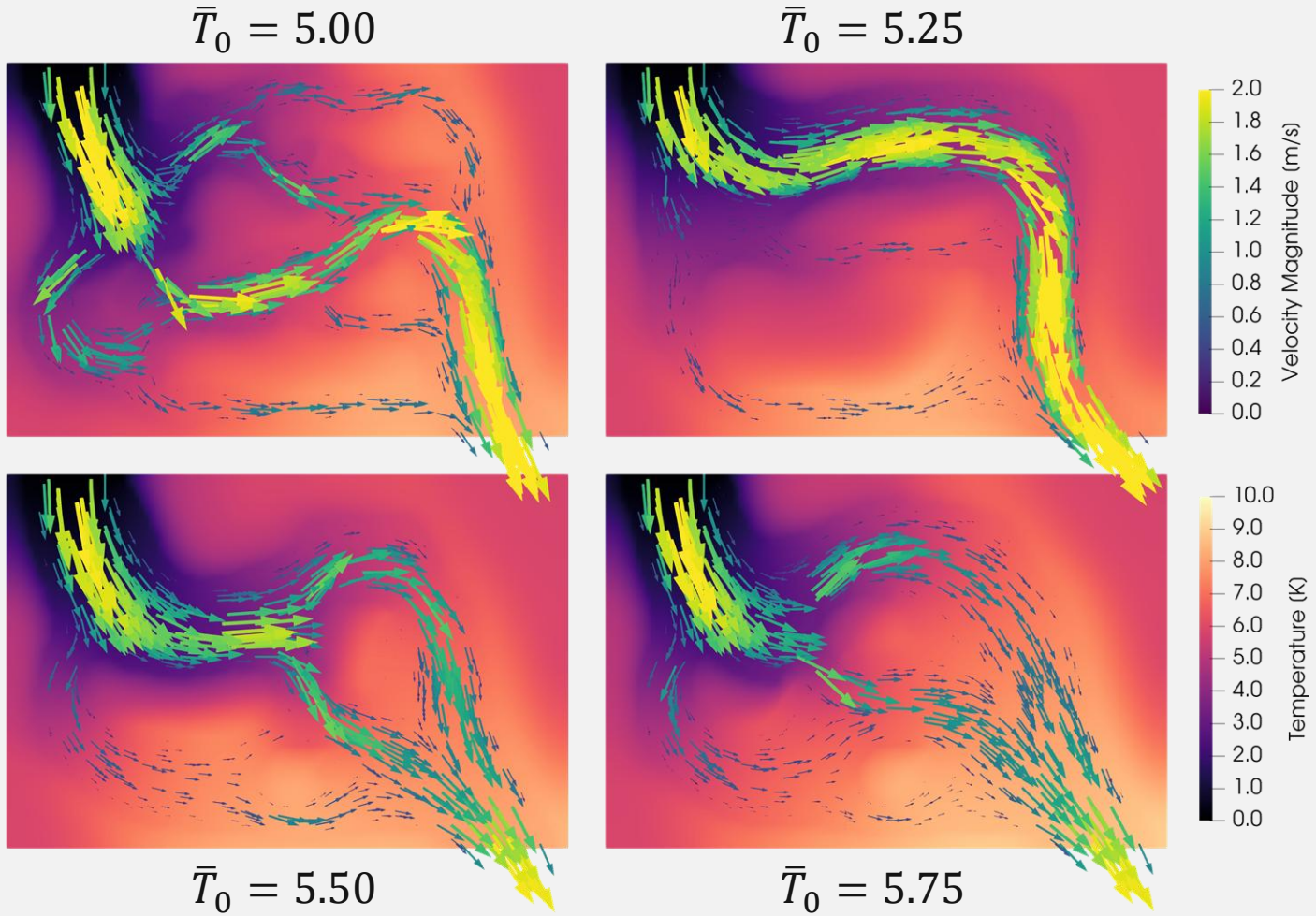

5.00 K: Narrow channels penetrate the PCM, reducing temperature at the cost of high pressure drop

5.25–5.50 K: Side-branches disappear, velocities drop slightly, creating minor warm spots

5.75 K: Wide channels dominate with uniform velocities yielding hotter corners but minimizing pressure drop

Influence of latent heat of fusion

$L_f = 40$

$L_f = 60$

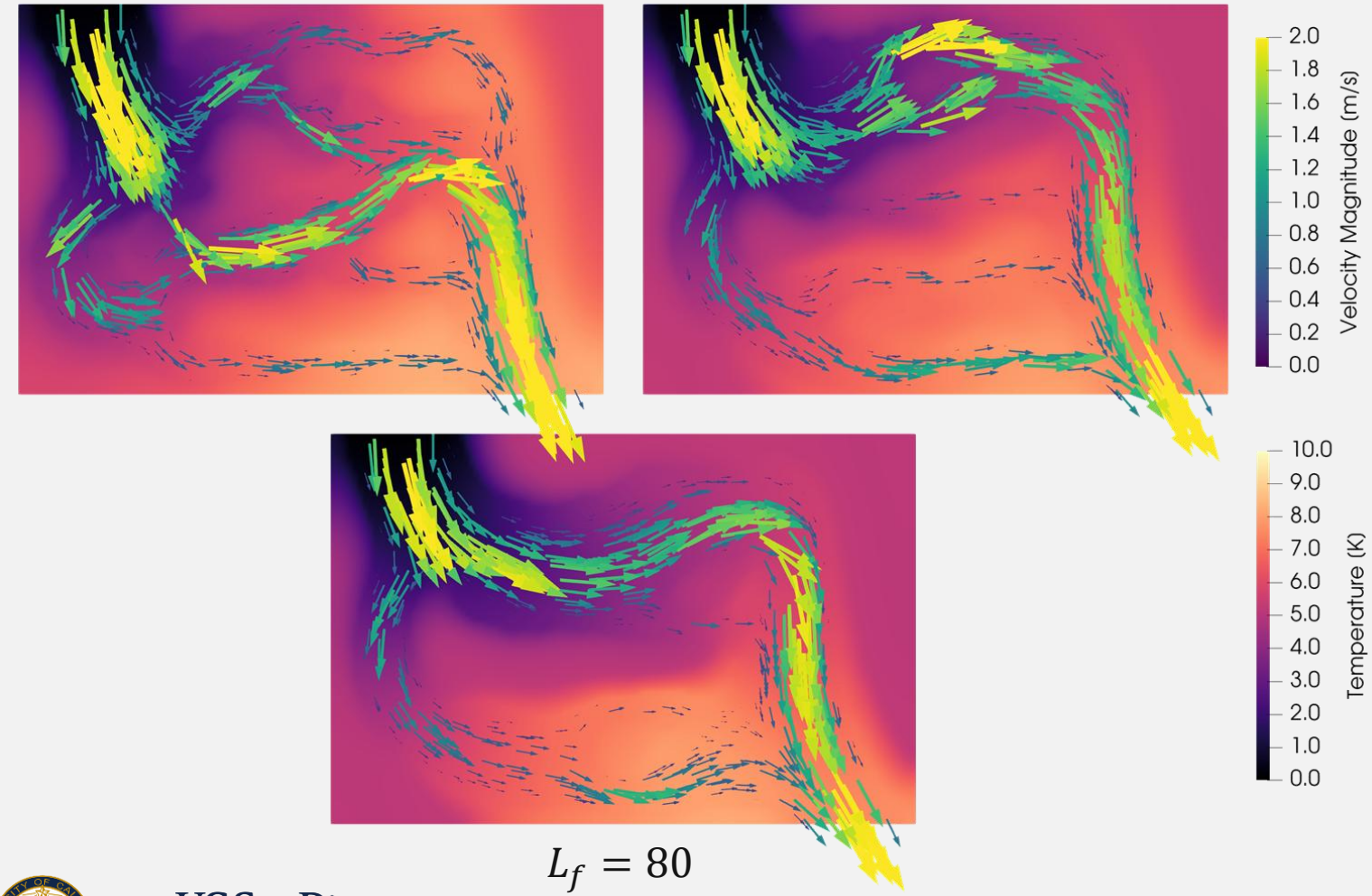

$L_f = 80$

$L_f = 40$: Branched channels drive cool fluid deep into the PCM yielding a relatively uniform temperature field

$L_f = 60$: Straighter parallel channels with hotter regions in weaker-flow zones near outlet

$L_f = 80$: Wide loop yields a hot spot near the outlet while greatly reducing pressure drop

Influence of latent heat of fusion

$L_f = 40$

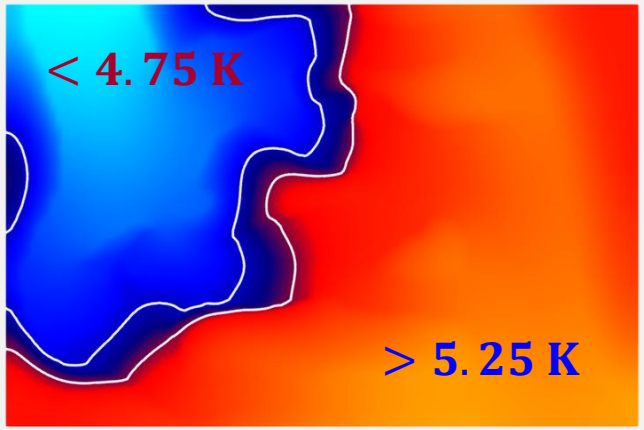

$L_f = 60$

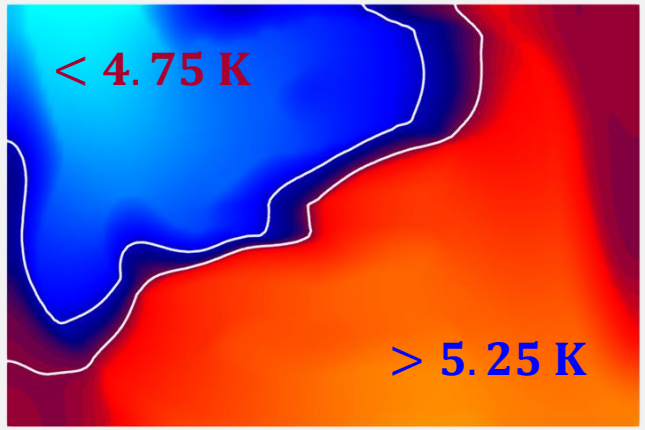

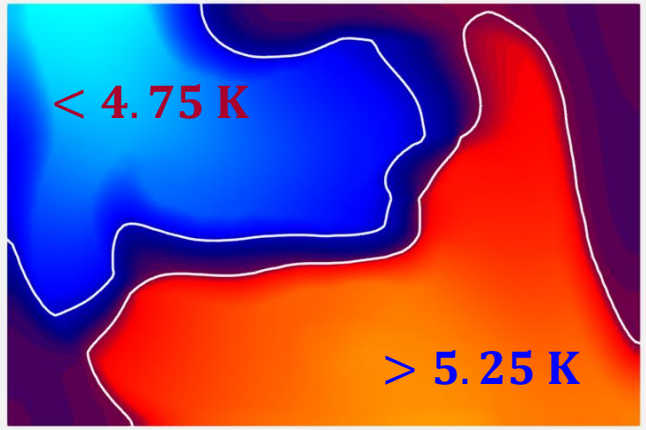

$L_f = 80$

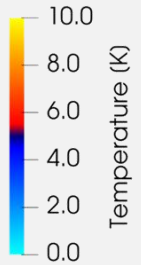

T < 4.75 K
→ solid PCM
T > 5.25 K
→ liquid PCM

$L_f = 40$
PCM volume fraction: 55%
Liquid fraction of PCM 64% ($T_{\mathrm{PCM}} > 5.25$ K)

$L_f = 60$
PCM volume fraction: 56%
Liquid fraction of PCM 63% ($T_{\mathrm{PCM}} > 5.25$ K)

$L_f = 80$
PCM volume fraction: 53%
Liquid fraction of PCM 33% ($T_{\mathrm{PCM}} > 5.25$ K)

→ Higher L_f reduces melt fraction despite similar PCM volumes